IOPscience iopscience.iop.org

Home Search Collections Journals About Contact us My IOPscience

Subpixel image stitching for linewidth measurement based on digital image correlation

This article has been downloaded from IOPscience. Please scroll down to see the full text article.

2010 Meas. Sci. Technol. 21 105104

(http://iopscience.iop.org/0957-0233/21/10/105104)

View the table of contents for this issue, or go to the journal homepage for more

Download details:
IP Address: 129.6.33.172
The article was downloaded on 17/08/2010 at 22:06

Please note that terms and conditions apply.

IOP PUBLISHING MEASUREMENT SCIENCE AND TECHNOLOGY

Meas. Sci. Technol. **21** (2010) 105104 (5pp) doi:10.1088/0957-0233/21/10/105104

Subpixel image stitching for linewidth measurement based on digital image correlation

Wei Chu, Joseph Fu and Theodore V Vorburger

National Institute of Standards and Technology, 100 Bureau Drive, Gaithersburg, MD 20899, USA

E-mail: wei.chu@nist.gov

Received 22 February 2010, in final form 29 June 2010
Published 13 August 2010
Online at stacks.iop.org/MST/21/105104

Abstract

The inevitable tilt angle resulting from attaching a carbon nanotube to an atomic force microscope (AFM) probe causes probe-related distortion on one sidewall of the linewidth sample during an AFM scan. In order to obtain accurate images at both sidewalls, an image stitching method was proposed in our previous research. An improved digital image correlation technique is outlined here to register two scanned images and detect the relative lateral distortion between them. Then image correction is performed pixel by pixel on both images prior to the stitching. A composite image is formed by stitching these two corrected images, and the linewidth is calculated based on this composite image. Since this method removes a significant portion of in-plane distortion between two images due to the nonlinearity of the AFM piezoelectric tube scanner, uncertainty in the calculation of linewidth due to the image stitching component is estimated to be reduced to the subpixel level from its former estimation of approximately three pixels. The procedure is tested with two standard linewidth features.

Keywords: linewidth, atomic force microscopy, carbon nanotube tip, image registration, image stitching, digital image correlation, nonlinearity, piezoelectric tube

(Some figures in this article are in colour only in the electronic version)

1. Introduction

Since 2004, the National Institute of Standards and Technology (NIST) and Harbin Institute of Technology (HIT), China, have collaborated on a study to apply image registration techniques to linewidth measurements [1] using atomic force microscopy (AFM). The purpose of this research is to reduce the image distortion of measurements at the sidewalls that can be introduced even with a fine carbon nanotube as the probe. Although nanotubes can detect information from deep trenches that conventional probes cannot, distortion at the sidewalls may result when a linewidth sample is scanned, particularly if there is any tilt in the mounted probe with respect to the surface normal. In that case, an accurate image of only one sidewall of the linewidth sample can be obtained, rather than both sidewalls. The slanted side of a nanotube cannot contact the sidewall entirely, and this leads to a distortion of the image, which seriously affects the measured value of the linewidth.

An image stitching method is proposed to resolve this problem. After the first image, which provides an accurate profile of one side of the measured line, is obtained, the sample is rotated 180° to obtain the second image, which provides an accurate profile for the other side of the line. The second image is then rotated back by 180°, and the two images are stitched to form a new image in which both sidewalls are minimally distorted.

An important issue for the image stitching approach is how to match the spatial position of two different scanned images using an effective image registration method. In previous research, the manual matching and the template matching methods were applied to the same experimental data to register images before stitching [2, 3]. The linewidth and its uncertainty were then estimated based on calculations using the stitched image. The template matching method can automatically implement this image registration processing, but this approach is restricted by the assumption of a rigid

 © 2010 IOP Publishing Ltd Printed in the UK & the USA

body transform between the two images, and it ignores any nonlinearities in the scanned images that may arise for example from the nonlinearities of piezoelectric tube (PZT) scanners. As a result of the simplification, the uncertainty of the image stitching approach was estimated to be approximately 3 pixels in a previous experiment. This was a large uncertainty component in the linewidth measurement. In this paper, an improved digital image correlation (DIC) technique is applied to reduce the uncertainty of the image stitching component to the subpixel level.

DIC was first conceived and developed in the early 1980s for application in the field of experimental mechanics [4–6]. It has become an accepted method for measuring surface displacements and displacement gradients in materials under deformation. Continuous optimization and improvement have been made after its initial development. In recent years, some researchers successfully extended its range of applications from the optical images of deformed surfaces to the distortion of AFM images [7–9].

However, most of these AFM applications are only concerned with the in-plane distortion, and do not take the out-of-plane distortion into account. Clearly, like the x- and y-motions, the z-motion of a PZT is also subject to nonlinear behavior. Fu, for example, encountered approximately a 6% nonlinearity variation in the z-motion of a PZT when different bias voltages were applied in a scan over a 100 nm step height sample [10]. When applied in the DIC method, calculations based on height information affected by PZT nonlinearity would decrease the accuracy of calculated in-plane displacement fields.

In the research of Vendroux and Knauss [11], the effect of an out-of-plane displacement on the calculation of the in-plane displacement field was considered for the first time. It was a simplified model which assumed that all vertical displacements in a local region were the same. It is not an accurate model since the stretch and contraction of the PZT along the z-direction are affected by drift, past history and other errors that change with time in a practical AFM scan. In the resulting AFM image, the error changes with lateral position. The final recorded z-direction height value is a sum of the real surface topography of the sample and the errors of motion of the PZT. In order to improve the accuracy of the displacement field calculations in a topographic image, an improved DIC method was proposed and tested on AFM images of compact discs [12]. The DIC method is tested further here as part of the image stitching approach for linewidth measurement that we are researching on prototypes of single crystal critical dimension reference materials (SCCDRMs) [13]. In this paper, the improved DIC method is briefly described in section 2, and its application to stitching measurements of linewidth is described in section 3.

2. Methodology for subpixel image registration

A subset of points S in a reference image around a grid point (x_0, y_0) is mapped to a subset $\tilde{S}$ in an in-plane deformed image. Correspondingly, each of the points (x, y) located in the subset S is mapped to the deformed image at the location $(\tilde{x}, \tilde{y})$ using

$$\tilde{x} = x + U(x, y), \qquad (1a)$$

$$\tilde{y} = y + V(x, y), \qquad (1b)$$

with U and V being the in-plane displacements of each subset point. We expand the functions U and V as Taylor series around (x_0, y_0) into

$$\tilde{x} = x + U(x_0, y_0) + \left.\frac{\partial U}{\partial x}\right|_{x_0,y_0}(x - x_0) + \left.\frac{\partial U}{\partial y}\right|_{x_0,y_0}(y - y_0) + \cdots, \qquad (2a)$$

$$\tilde{y} = y + V(x_0, y_0) + \left.\frac{\partial V}{\partial x}\right|_{x_0,y_0}(x - x_0) + \left.\frac{\partial V}{\partial y}\right|_{x_0,y_0}(y - y_0) + \cdots. \qquad (2b)$$

Theoretically, expanding into higher order Taylor series yields higher precision, but if the subset is sufficiently small, a first-order expansion is sufficiently accurate and is adopted by most researchers using the DIC method.

Let $\mathbf{P}$ represent an array of parameters of the mapping from S to $\tilde{S}$; let $f(x, y)$ and $g(x, y, \mathbf{P})$, or $g(\tilde{x}, \tilde{y})$, represent the reference image and the deformed image, respectively, and let S_p represent any single point in the subset. Thus the value of $f(x, y)$ at the point S_p can be written as $f(S_p)$, and the value of $g(\tilde{x}, \tilde{y})$ at the counterpart of S_p can be written as $g(S_p, \mathbf{P})$. We use the sum of squared intensity differences, denoted as C, to quantify how well the two subsets match:

$$C = \sum_{S_p \in S} [f(S_p) - g(S_p, \mathbf{P})]^2. \qquad (3)$$

If we ignored the differences in the vertical direction and assumed that there was only lateral distortion between two images to be compared, $\mathbf{P}$ would only consist of six unknown parameters, i.e. $U(x_0, y_0)$, $V(x_0, y_0)$, $\left.\frac{\partial U}{\partial x}\right|_{x_0,y_0}$, $\left.\frac{\partial U}{\partial y}\right|_{x_0,y_0}$, $\left.\frac{\partial V}{\partial x}\right|_{x_0,y_0}$ and $\left.\frac{\partial V}{\partial y}\right|_{x_0,y_0}$ as in equation (1b). Since the DIC method is conceived to find an optimum $\mathbf{P}$ for minimizing C by solving an optimization problem, we hereafter use the functions $[U\ V\ \frac{\partial U}{\partial x}\ \frac{\partial U}{\partial y}\ \frac{\partial V}{\partial x}\ \frac{\partial V}{\partial y}]$ to replace the original six components of $\mathbf{P}$.

As we described above, the nonlinearity error of a PZT in the z-direction should not be ignored. So the height value of a deformed image is modified and formulated as equation (4). By approximating the error in the z-direction to be linear within a sufficiently small area, three more parameters are added: the parameter w_0 represents a constant height difference between S and $\tilde{S}$, w_1 represents the coefficient of variation of PZT length with scanning position along the x-direction and w_2 stands for that along the y-direction. Thus $g(S_p, \mathbf{P})$ in equation (3) will be replaced by $\tilde{g}(S_p, \mathbf{P})$ below:

$$\tilde{g}(S_p, \mathbf{P}) = g(S_p, \mathbf{P}) + w_0 + w_1(x - x_0) + w_2(y - y_0). \qquad (4)$$

To find the minimum of C, the gradient of C with respect to variation in the parameters must be zero. Let p_i ($i = 1, \ldots, 9$) denote U, V, $\frac{\partial U}{\partial x}$, $\frac{\partial V}{\partial x}$, $\frac{\partial U}{\partial y}$, $\frac{\partial V}{\partial y}$, w_0, w_1, w_2. We have

$$\nabla C = -2 \times \left\{ \sum_{S_p \in S} [f(S_p) - \tilde{g}(S_p, \mathbf{P})] \frac{\partial \tilde{g}(S_p, \mathbf{P})}{\partial p_i} \right\}_{i=1,\ldots,9} = 0. \qquad (5)$$

Figure 1. AFM scanning image of the linewidth sample: (*a*) reference image; (*b*) rotated image (after 180° sample rotation and 180° image rotation). The image area is about 2.3 μm × 2.3 μm.

The nonlinear equation can be solved using the Newton–Raphson iteration method. Therefore, we can obtain

$$\mathbf{P}^{k+1} = \mathbf{P}^k - \nabla C(\mathbf{P}^k) \cdot [\nabla\nabla C(\mathbf{P}^k)]^{-1}, \quad (6)$$

where $\mathbf{P}^k$ is the kth iteration value and $\mathbf{P}^{k+1}$ is the approximation value after the $(k + 1)$st iteration. $\nabla\nabla C(\mathbf{P})$ is the Hessian matrix [14]:

$$\nabla\nabla C(\mathbf{P}) = \left(\frac{\partial^2 C}{\partial p_i \partial p_j}\right)_{i=1,\ldots,9;\, j=1,\ldots,9}. \quad (7)$$

Once the iteration is completed, the final values of the functions U and V in $\mathbf{P}$ can be viewed as the position discrepancy of the point (x_0, y_0) along the x- and y-directions between two images, i.e. $U(x_0, y_0)$, $V(x_0, y_0)$. The displacement fields U and V for all pixel points will be formed by moving the subset S pixel by pixel.

3. Image stitching and experiment

The same experimental data used in our previous study [3] are used here to generate registration results using the improved DIC method and subsequent image stitching processing. Figures 1(*a*) and (*b*) are the images of the first and the second scan, which are measured before and after rotating the linewidth sample by 180°.

Taking the image acquired before sample rotation as the reference, a window consists of a 41 × 41 pixel area that moves around the whole reference image. For a certain window position with an initial guess of $\mathbf{P}$, there is a corresponding deformed subarea in the rotated image. All data points in the deformed subarea are one-to-one mapped from the window in the reference image. The positions and z-values of all these data points will be reconstructed based on interpolation of the rotated image and the initial value of $\mathbf{P}$. An iteration process is performed as described in the previous section until the change in the sum of squared intensity differences C is smaller than a certain threshold. During the iteration process, the positions and z-values of all points inside the deformed subarea in the rotated image are adjusted with the changes in $\mathbf{P}$. When the iteration is complete, a best-matching deformed subarea in the rotated image is determined by an optimum $\mathbf{P}$. Finally, a nine-component $\mathbf{P}$ array will be obtained for each point in the reference image, except for those points located near the borders.

Two components of $\mathbf{P}$, the displacement fields U and V, are shown in figure 2. The image areas are smaller than the original images after removal of the non-overlapping areas of the two images and 20 pixels of the border areas. From the field images, a number of vacant points that do not have valid displacement values can be seen. Most of these points are located near the two sidewall areas where large differences between the two topographic images occur because an accurate image of only one sidewall of the linewidth sample can be obtained from each image. Those large differences cause the iteration calculation for the subset areas around these points to diverge and to show up as vacant points in figure 2. In addition, other outlier points yield unreliable displacement values which differ markedly from those of their neighbors. They account for about 1% of the total data points. Interpolation from neighboring points is then performed to fill up the vacant points.

After these exclusion and interpolation processes, the displacement fields between the first and second scanned images are obtained. However, we do not know which image is closer to the actual sample topography. Therefore the corrected positions of the data points are obtained by splitting the differences between the images. With an assumption that the reference and rotated images take half the value of the displacement fields as their distortion from the real sample, both images are corrected by adjusting only their respective in-plane (x–y) positions by the same distance in opposite directions for each pixel.

4. Results and discussion

We combine the right side of the reference image and the left side of the rotated image to form a new image, as shown in figure 3. The same pair of raw data has been used to generate three stitched composite images with three different image registration methods: manual operation, template matching and the DIC method. The measurement results calculated from the stitched images for two samples are listed in table 1.

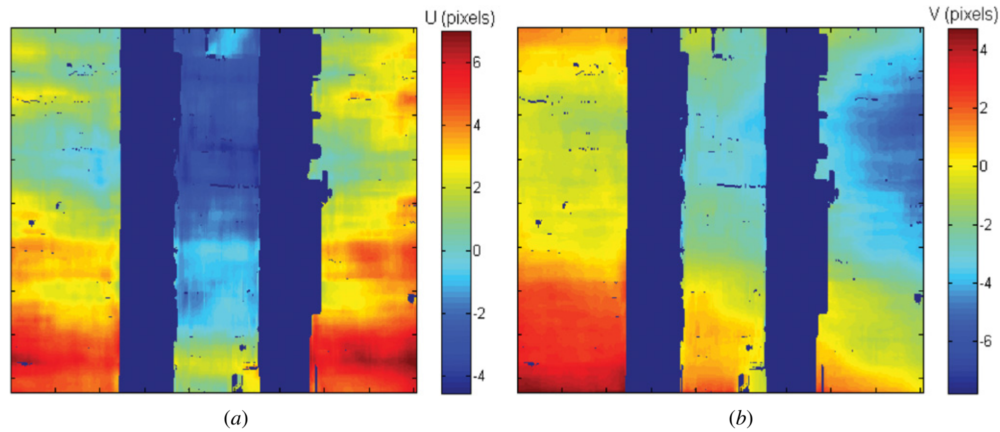

(*a*) (*b*)

Figure 2. Displacement fields between two images: (*a*) *U* field in the horizontal/fast scan direction; (*b*) *V* field in the vertical/slow scan direction. The dark areas mostly located near the two sidewalls of the sample represent invalid displacement data. The image areas are about 2.1 μm wide and 2.0 μm high.

Figure 3. Stitched image. The image area is about 2.1 μm wide and 2.0 μm high.

Table 1. Comparison of the linewidth calculation results using different registration methods and a CD-AFM. The linewidths are calculated between points near the top of the line just below the corner. The data for sample 2 are shown in figures 1–3.

	Manually (nm)	Template matching (nm)	DIC (nm)	CD-AFM (nm)
Sample 1	536.6	535.4	536.3	557.1
Sample 2	574.9	563.4	564.0	577.5

The linewidths calculated from the stitched images obtained here with template matching differs from that reported in our earlier publication, where template matching was also used [3], because different edge definitions are used here. In the earlier experiment, the step edge was determined by a linewidth model and an algorithm [15]. In order to be consistent with the manual stitching operation [2] and avoid the methodological error that comes from a different edge definition, that model is not adopted for linewidth calculation in this paper.

Another pair of images, which was available from our previously reported manual matching study, is registered again using template matching and DIC methods for generating composite images and calculating the linewidth.

Repeating the DIC method over the two corrected images, the average absolute value of the new *U* and *V* fields are only 0.30 pixels and 0.14 pixels. This result suggests that the DIC method provides stable, repeatable results for image correction and registration. We conservatively estimate the standard uncertainty from our image stitching calculation to be about 1 pixel, or 4.5 nm. This is a significant improvement compared with our previous estimate of about 3 pixels, or 13.5 nm, where the nonlinear distortion in the AFM-scanned images was neglected.

The standard linewidth features of the prototype SCCDRMs were fabricated by preferential KOH etching of {1 1 0} silicon. Consequently, the sidewalls are aligned with {1 1 1} planes and thus have sidewall angles defined by the crystallography to be very close to 90°. The manufacturing details of these structures can be found elsewhere [15]. Their linewidths as measured with a critical dimension atomic force microscope (CD-AFM) [16] are also listed in table 1 for comparison. NIST's CD-AFM provides traceable linewidth metrology for semiconductor manufacturing. The uncertainty for linewidth measurement with the CD-AFM is approximately 2 nm ($k = 2$). The average difference between the image stitching results and the CD-AFM results is approximately 17.2 nm as shown in table 1. A number of other sources of bias and uncertainty besides that due to the stitching calculation need to be investigated. We have previously [3] estimated standard uncertainties due to an AFM scale calibration of 1% (7 nm), a tip diameter uncertainty of 8 nm and a bias due to a tip compliance of 3 nm assuming Lennard–Jones forces [17]. Other potential sources of error not yet estimated include scanner errors common to both images, tip compliance due to capillary forces, algorithmic differences between the calculation of linewidth from this work and from the CD-AFM, and room temperature variations [18]. Since all those uncertainty components are independent of each other, the final combined uncertainty would be determined by their root sum square.

Acknowledgment

The authors are grateful to R Dixson of NIST for providing the measurement data for the linewidth samples using a CD-AFM and for some helpful discussions.

References

[1] Zhao X, Fu J, Chu W, Nguyen C and Vorburger T 2004 An image stitching method to eliminate the distortion of the sidewall in linewidth measurement *Proc. SPIE* **5375** 363–73

[2] Fu J, Dixson R, Orji G, Vorburger T and Nguyen C 2005 Linewidth measurement from a stitched AFM image *Characterization and Metrology for ULSI Technology* (*Richardson, TX, USA, 15–18 March*) vol 788 (Melville, NY: AIP) pp 421–6

[3] Chu W, Fu J, Dixson R and Vorburger T 2007 Linewidth measurement based on automatically matched and stitched AFM images *Int. Conf. Frontiers of Characterization and Metrology (Gaithersburg, MD, USA, 27–29 March)* vol 931 (Melville, NY: AIP) pp 407–12

[4] Chu T C, Ranson W F, Sutton M A and Peters W H 1985 Applications of digital-image-correlation techniques to experimental mechanics *Exp. Mech.* **25** 232–44

[5] Bruck H A, McNeill S R, Sutton M A and Peters W H III 1989 Digital image correlation using Newton–Raphson method of partial differential correlation *Exp. Mech.* **29** 261–7

[6] Sutton M A, McNeill S R, Helm J D and Chao Y J 2000 Advances in two-dimensional and three-dimensional computer vision *Photomechanics (Topics in Applied Physics)* vol 77 (Berlin: Springer) pp 323–72

[7] Chang S, Wang C S, Xiong C Y and Fang J 2005 Nanoscale in-plane displacement evaluation by AFM scanning and digital image correlation processing *Nanotechnology* **16** 344–9

[8] Jin H and Bruch H A 2005 A new method for characterizing nonlinearity in scanning probe microscopes using digital image correction *Nanotechnology* **16** 1849–55

[9] Sun Y and Pang J H L 2006 AFM image reconstruction for deformation measurements by digital image correlation 2006 *Nanotechnology* **17** 933–9

[10] Fu J 1995 *In situ* testing and calibrating of z-piezo of an atomic force microscope *Rev. Sci. Instrum.* **66** 3785–8

[11] Vendroux G and Knauss W G 1998 Submicron deformation field measurements: part 2. Improved digital image correlation *Exp. Mech.* **38** 86–92

[12] Chu W, Fu J and Vorburger T 2009 An improved digital image correlation method applied to scanning probe microscope images *Int. Manufacturing Science and Engineering Conf. (West Lafayette, IN, USA, 4–7 October)*

[13] Allen R A, Am Ende B A, Cresswell M W, Murabito C E, Headley T J, Guthrie W F, Linholm L W, Ellenwood C H and Bogardus E H 2003 Test structures for referencing electrical linewidth measurements to silicon lattice parameters using HRTEM *IEEE Trans. Semicond. Manuf.* **16** 239–48

[14] Neudecker H and Magnus J R 1988 *Matrix Differential Calculus with Applications in Statistics and Econometrics* (New York: Wiley)

[15] Zhao X, Vorburger T, Fu J, Song J and Nguyen C 2003 A model for step height, edge slope and linewidth measurements using AFM *Int. Conf. Characterization and Metrology for ULSI Technology (Austin, TX, USA, 24–28 March)* vol 683 (Melville, NY: AIP) pp 400–8

[16] Dixson R, Fu J, Orji N, Guthrie W, Allen R and Cresswell M 2005 CD-AFM reference metrology at NIST and SEMATECH *Proc. SPIE* **5752** 324–36

[17] Feng S C, Vorburger T, Joung C B, Dixson R, Fu J and Ma L 2008 Computational models of the nano probe tip for static behaviors *Scanning* **30** 47–55

[18] Fu J, Chu W and Vorburger T 2009 Influence of room temperature control on atomic force microscope imaging *J. Vac. Sci. Technol.* B **27** 2321–3